Ir(III)-based Ratiometric Hypoxic Probe for Cell Imaging

Shi-Lu Ji[a,b], Hua-Min Lan[a], Sen-Sen Zhou[a], Xiao-Ke Zhang[a], Wei-Zhi Chen[a*], and Xi-Qun Jiang[a*]

[a] *Department of Polymer Science & Engineering, College of Chemistry & Chemical Engineering, Nanjing University, Nanjing 210093, China*
[b] *College of Science, Nanjing Forestry University, Nanjing 210037, China*

Ⓔ Electronic Supplementary Information

Abstract Two new ratiometric hypoxia probes (Ir-C343 and Ir-GFP) are synthesized by covalently incorporating florescent internal standard molecules coumarin 343 (C343) and green fluorescent protein (GFP) into bis[1-(9,9-dimethyl-9*H*-fluoren-2-yl)-isoquinoline] (succinylacetone) Ir(III) (Ir-fliq), respectively. After connecting with internal standard molecules, the Ir-fliq moiety still exhibits high sensitivity to oxygen concentration, while the fluorescence intensity of the internal standard remains relatively constant under different oxygen concentrations. As a result, a ratiometric response is realized that is only related to oxygen concentration. In addition, Ir-GFP shows more promising applications in the ratiometric hypoxia imaging of cells due to its long excitation wavelength, good water solubility, high biocompatibility, and low relative fluorescence intensity compared with the phosphorescent emitter Ir-fliq.

Citation: Ji, S. L.; Lan, H. M.; Zhou, S. S.; Zhang, X. K.; Chen, W. Z.; Jiang, X. Q. Ir(III)-based ratiometric hypoxic probe for cell imaging. *Chinese J. Polym. Sci.* **2023**, *41*, 794–801.

INTRODUCTION

Exploring physiological and pathological changes is of great importance for diagnosis and treatment of diseases.[1,2] In recent years, optical imaging technologies have made significant progress in biomedical field, especially the emergence of various functional optical probes with high sensitivity, good specificity, simple and fast operation. They have the capacities to image molecules, cells, tissues and even organs in a non-invasive, real-time and dynamic manner.[3] With the rapid development of materials science and nanotechnology, several new types of optical probes have been reported, and they have made great breakthroughs in the field of *in vitro* and *in vivo* imaging.

Among a variety of new optical probes, nanoprobes have attracted extensive research attention recently. Compared to traditional small molecule probes, nanoprobes exhibit improved sensitivity, good specificity and targeting capabilities of optical imaging due to their inherent optical and physicochemical properties.[4–7] However, there are still some challenges in the practical applications of optical nanoprobes. Conventional optical probes rely on a signal transduction mode, in which the target molecule is detected and imaged by turning the signal 'on' or 'off'. However, the intensity-dependent signal captured by a single-targeted optical probe may be affected by experimental, environmental or physiological factors, which are unrelated to the concentration of the target. Typical examples of these factors include the following: (1) inhomogeneous delivery and insufficient elution; (2) changes in mechanical properties, permeability and retention between healthy and diseased tissues; (3) instrumentation variables such as detection distance and illumination angles; and (4) chemical binding or capture of the probe molecules by non-targets in the tissue.[8–11] These factors can lead to non-specific and grossly misleading imaging and result in false-positive results. Currently, these issues have become a major obstacle to the use of single-target probes in conventional molecular imaging.

Oxygen is one of the most important elements for life. Designing hypoxia probes for the determination of oxygen content in cells or tissues is extremely important. In practice, intensity-dependent signals based on a single hypoxia probe are susceptible to interference from probe concentration, light scattering and external environment (such as temperature or pH). What's more, it is difficult to determine the oxygen concentration accurately without complex data processing. Because pO_2 and fluorescence intensity are often not linearly dependent.[12]

To address these challenges, researchers have proposed a variety of approaches to mitigate the effects of non-specific background signals, including the use of dual tracer deduction[13] and paired detection groups.[14] Among the available methods, a simple and effective way to reduce the effect of non-specific signals is to capture ratiometric signals instead of intensity-dependent signals. Ratiometric probes can be self-

calibrated by recording signal fluctuations caused by two or more analysis targets, where one of the non-specific signals can be used as a reference standard for the target signal.[15–17] Ratiometric measurements do not depend on local probe concentrations or various other factors unrelated to the analysed target. Therefore, optimizing optical probes using ratiometric measurements is a valuable imaging method that can improve the ability to monitor physiological or pathological processes, increase the effectiveness of disease diagnosis and treatment, and accelerate the process of clinical translation of probes.

In order to achieve low-interference and high-efficiency optical imaging, two types of ratiometric probes based on Ir-fliq were designed to achieve ratiometric hypoxia imaging at the cellular level. Iridium complexes have been widely used in organic light-emitting devices (OLEDs) field[18–21] and are expected to be further used in biological imaging due to their superior optical properties. However, traditional Ir complexes are generally hydrophobic and have non-negligible cytotoxicity.[22] For this reason, we hope to develop Ir probes with good water solubility and negligible toxicity. First, the Ir-C343 ratiometric probe was synthesized using coumarin 343 (C343) as an internal standard probe to quantify the difference in signals between cells at different oxygen concentrations. However, the Ir-C343 probe suffers from poor water solubility, bad biocompatibility and short excitation wavelength of the internal standard molecule C343. To address these issues, we further construct a Planck F127-coated nanoparticles Ir-C343@F127 that shows improved water solubility and biocompatibility. Subsequently, green fluorescent protein (GFP) was introduced to replace C343 as the internal standard molecule to synthesize ratiometric probe Ir-GFP. Our current work shows Ir-GFP can realize the ratiometric imaging of common cells due to its good biocompatibility, and has very promising applications in the study of single-cell respiratory metabolism.

EXPERIMENTAL

Reagents and Materials
Iridium chloride hydrate, 2-ethoxyethanol, 1-chloroisoquinoline, 1,3,2-dioxaborolane, sodium hydride, levulinic acid, 1-boc-piperazine, N-α-carbobenzoxy proline, coumarin C343, 1-ethyl-(3-dimethylaminopropyl) carbodiimide (EDC), N-hydroxysuccinimide (NHS), 2-(1H-7-azabenzotriazol-1-yl)-1,1,3,3-tetramethylammonium hexafluorophosphate (HBTU), 2-(N-morpholinyl) ethanesulfonic acid and Pluronic F127 were purchased from Sigma-Aldrich. All these chemicals were used directly without further purification.

Cell Lines
Mouse mononuclear macrophages (RAW264.7) and mouse embryonic fibroblasts (NIH3T3) were provided by the Shanghai Institute of Cell Biology. $E.\ coli$ TOP10 and BL21 strains were purchased from Tiangen Biochemical Technology Co.

Testing Instruments and Methods
Nuclear magnetic resonance spectra (^{1}H-NMR) were measured with a Bruker DRX-400 NMR spectrometer. Mass spectra were acquired by the LCQ ESI-MS Therso Finnigan mass spectrometer. Protein mass were measured with a matrix-assisted laser desorption ionization time of flight mass spectrometer (MALDI-TOF/TOF Mass Spectrometer). Emission spectra were obtained with a HORIBA FL-3 fluorescence spectrometer. $In\ vitro$ cytotoxicity assay was performed by a TECAN Infinite M200 Pro multifunctional enzyme marker and the laser confocal imaging of cells was taken by Zeiss LSM-710.

Synthesis of the Ratio-based Probe Ir-C343

Synthesis of Ir-fliq
A small molecule probe Ir-fliq (**11**) and a macromolecular molecule probe Ir-fliq-PVP (**12**) based on iridium complexes were synthesized according to the method reported previously.[23] We chose 1-(9,9-dimethyl-9H-fluoren-2-yl) isoquinoline (fliq) as the main ligand and succinyl acetone (sa) as the ancillary ligand. The synthetic route is shown in Fig. S1 (in the electronic supplementary information, ESI).

Synthesis of tetraproline-coumarin (Pro₄-C343)
According to the method reported before,[24] the amidation reaction occurred between the amino group of 1-boc-piperazine and the carboxyl group of N-α-carbobenzoxy proline. After debenzylation, the amino group obtained could continue to react with the carboxyl group on proline. This process was repeated four times to obtain H-Pro₄-Pipe-Boc. Afterwards, it was linked to the internal standard probe C343. The synthetic route is shown in Fig. S2 (in ESI).

Synthesis of the ratiometric probe Ir-C343
As shown in Fig. S3 (in ESI), Pro₄-C343, Ir-fliq (99.1 mg, 0.1 mmol) and HBTU (55 mg, 0.15 mmol) were dissolved in anhydrous DMF (10 mL) followed by the addition of N,N-diisopropyl ethylamine (0.04 mL). After stirred for 1 h at 0 °C and 20 h at room temperature, pure water was added. The brown insoluble product was filtered off and purified by alumina column chromatography with chloroform:ethyl acetate (1/1, V/V) and silica column chromatography with chloroform:methanol (9/1, V/V) as eluents, respectively. Distilled under reduced pressure to remove the solvent to give Ir-C343 as an orange-yellow powder.

Preparation of Ir-C343 nanoparticles
In order to improve the water solubility of the ratiometric probe Ir-C343, the amphiphilic polymer Planck F127 was used to wrap Ir-C343 to prepare nanoparticles. F127 (35 mg) and Ir-C343 (1 mg) were dissolved in tetrahydrofuran (1 mL) and then dropped into water (9 mL) slowly under sonicated for 10 min. The mixture was dialyzed overnight and lyophilized to obtain Ir-C343@F127 nanoparticles.

Synthesis of the Ratiometric Probe Ir-GFP
Ir-fliq (50 mg, 0.05 mmol), EDC (10 mg, 0.052 mmol) and NHS (5.8 mg, 0.05 mmol) were dissolved in DMSO (5 mL) and stirred for 1 h to activate the carboxyl group on the ancillary ligand sa. The mixture was slowly added to GFP solution (135 mg, 0.005 mmol, 10 mL) dropwise and stirred at 4 °C in dark place for 24 h. The mixture was filtered to remove insoluble substances and lyophilized to obtain the water-soluble ratiometric probe Ir-GFP.

The mass spectra of GFP before and after the reaction with the small molecule probe Ir-fliq were obtained using a matrix-assisted laser desorption ionization time of flight mass spectrometer (MALDI-TOF/TOF Mass Spectrometer).

Cell Toxicity Test
The $in\ vitro$ cytotoxicity of the ratiometric probes Ir-C343, Ir-

C343@F127 and Ir-GFP was tested by MTT assay. RAW264.7 cells were inoculated in 96-well plates at a density of 5000/well at 37 °C with 5 % CO_2 for 24 h. After the cells were fully adhered, the culture medium was removed and 200 μL of medium containing different concentrations of the probe solution was added to each well. The final concentrations of Ir-fliq of the probes Ir-C343 and Ir-C343@F127 were 5, 10, 20, 30, 40 and 50 μg/mL. The final concentrations of Ir-GFP were 0.1, 0.2, 0.4, 1, 2 and 4 mg/mL. Six replicate wells were set up for each concentration. After 24 h of incubation, the culture medium was removed, and 180 μL of medium and 20 μL of MTT in PBS (5 mg/mL) were added to each well. After 4 h of incubation, the yellow MTT was reduced by the live cells to violet crystalline methylzan. The solution was removed from the wells and 150 μL of DMSO was added and dissolved for 10 min in dark place. The absorbance values at 570 nm were measured using a TECAN Infinite M200 Pro multifunctional enzyme marker. Calculate the cell viability.

Hypoxia Response Test with the Ratiometric Probes
The probe Ir-C343 was dissolved in DMSO (15 μg/mL) and the probe Ir-GFP was dissolved in water (0.3 mg/mL). Put the solution into a screw-top quartz four-way cuvette. Adjust the ratio of nitrogen and oxygen to different ratios by a flowmeter, and bubble to the bottom of the solution through the needle for 15 min to reach the equilibrium. Then the cuvette was sealed immediately with the lid. The emission spectra of the probes were measured at different oxygen concentrations. The excitation wavelength was 445 nm (Ir-C343) and 475 nm (Ir-GFP), respectively.

In vitro Cell Imaging with the Ratiometric Probes
NIH3T3 cells were incubated at 37 °C with 5% CO_2 for 24 h. DMSO solution of the probe Ir-C343 was added to the medium to a final concentration of 15 μg/mL. Co-incubate for 4 h, and then incubate in air or in an MGC AnaeroPack-Anaero hypoxic bag for 1 h. The signal was captured by a Zeiss LSM 710 laser confocal fluorescence microscope to test the probe's capability for the imaging of cells in hypoxia. The excitation wavelength was 405 nm and the signal detection range were 460−560 and 620−750 nm for the two channels, respectively.

RAW264.7 and NIH3T3 cells were co-incubated with Ir-GFP probe (0.3 mg/mL) for 4 h at different oxygen concentrations of 0% and 21%, respectively. The signal was captured by a Zeiss LSM 710 laser confocal fluorescence microscope. The excitation wavelength was 488 nm and the signal detection ranges were 505−550 and 620−750 nm for the two channels, respectively.

RAW264.7 cells were co-incubated with Ir-GFP probe (0.3 mg/mL) for 4 h. Then the medium was removed. Wash with PBS three times and a small amount of PBS was added. Lipopolysaccharide (LPS) solution (200 ng/mL) was added to one of the dishes and incubated for 1 h in a sealed incubator.

The signal was captured by a Zeiss LSM 710 laser confocal fluorescence microscope. The excitation wavelength was 488 nm, and the signal detection ranges were 505−550 and 620−750 nm for the two channels, respectively.

Preparation of Single-cell Microwells Array
The silicon mould used for the single-cell microwells array with the size of 30 μm was obtained from the group of Prof. Dechen

Jiang (Nanjing University). 5 μL of anti-plastering aid was added into a desiccator. Evacuate for 10 min and hold for 30 min to silanize the surface of the silicon mould. PDMS films were prepared using an adhesive of AB glue (10:1). The adhesive was stirred well and vacuumed for 10−20 min to remove air bubbles in the glue. Pour the adhesive evenly onto the surface of the silicon mould. Place the mould in an oven at 60 °C for 1 h to allow the adhesive to solidify into a film. Remove the film and place it upside down on a slide to be used as a single-cell microwell array.

Single-cell Imaging with Ir-GFP
The individual RAW264.7 cells were cultured at the microwell array with the probe Ir-GFP (0.3 mg/mL) for 2 h. The signal was captured by a Zeiss LSM 710 laser confocal fluorescence microscope. The excitation wavelength was 488 nm, and the signal detection ranges were 505−550 and 620−750 nm for the two channels, respectively.

RESULTS AND DISCUSSION

Synthesis and Optical Property of the Probes
We synthesized ratiometric probes Ir-C343 (Fig. 1a) and Ir-GFP (Fig. 1c), respectively, based on the iridium complex probe Ir-fliq. Their structures were confirmed by MS (Figs. S3 and S4 in ESI). As shown in Fig. 1(b), when excited at 445 nm, both the fluorescence peak of C343 at 550 nm and the phosphorescence peak from Ir-fliq at 670 nm can be observed. After exposed to the atmosphere with different oxygen concentrations, the fluorescence intensity at 550 nm remained constant, while the phosphorescence intensity at 670 nm significantly increased under hypoxic condition compared to that under normoxic conditions. It can be seen that Ir-C343 exhibits a good ratiometric hypoxia response, and the fluorescence emission peak at 550 nm can be as an internal standard to eliminate the influence of the probe concentration. The ratio of intensity at 670 and 550 nm is only related to the oxygen concentration and is independent of the probe concentration.

The molecular weights of GFP and Ir-GFP measured by MALDI-TOF are about 27741 and 29592 respectively (Fig. S4 in ESI), which proved that two Ir-fliq molecules were grafted to each GFP molecule on average. Since GFP has strong absorption at 475 nm, we chose 475 nm as the excitation wavelength, which is more suitable for subsequent applications in biological imaging. As shown in Fig. 1(d), two emission peaks are observed when excited at 475 nm, which correspond to the fluorescence peak at 510 nm from GFP and the phosphorescence peak at 670 nm from Ir-fliq, respectively. When exposed to the atmosphere with different oxygen concentrations, the fluorescence intensity at 550 nm remains unchanged, while the ratio of the phosphorescence intensity at 670 nm under hypoxic and oxygen-saturation conditions reaches about 2.0. Clearly, Ir-GFP also has a good ratiometric hypoxia response effect. Furthermore, Fig. 1(d) shows that the intensity of the fluorescence emission peak at 550 nm is much lower than the phosphorescence intensity of the Ir-fliq part, which may be more conducive to the study of the oxygen-sensitive phosphorescence peak.

Morphology Characterization of Nanoparticles
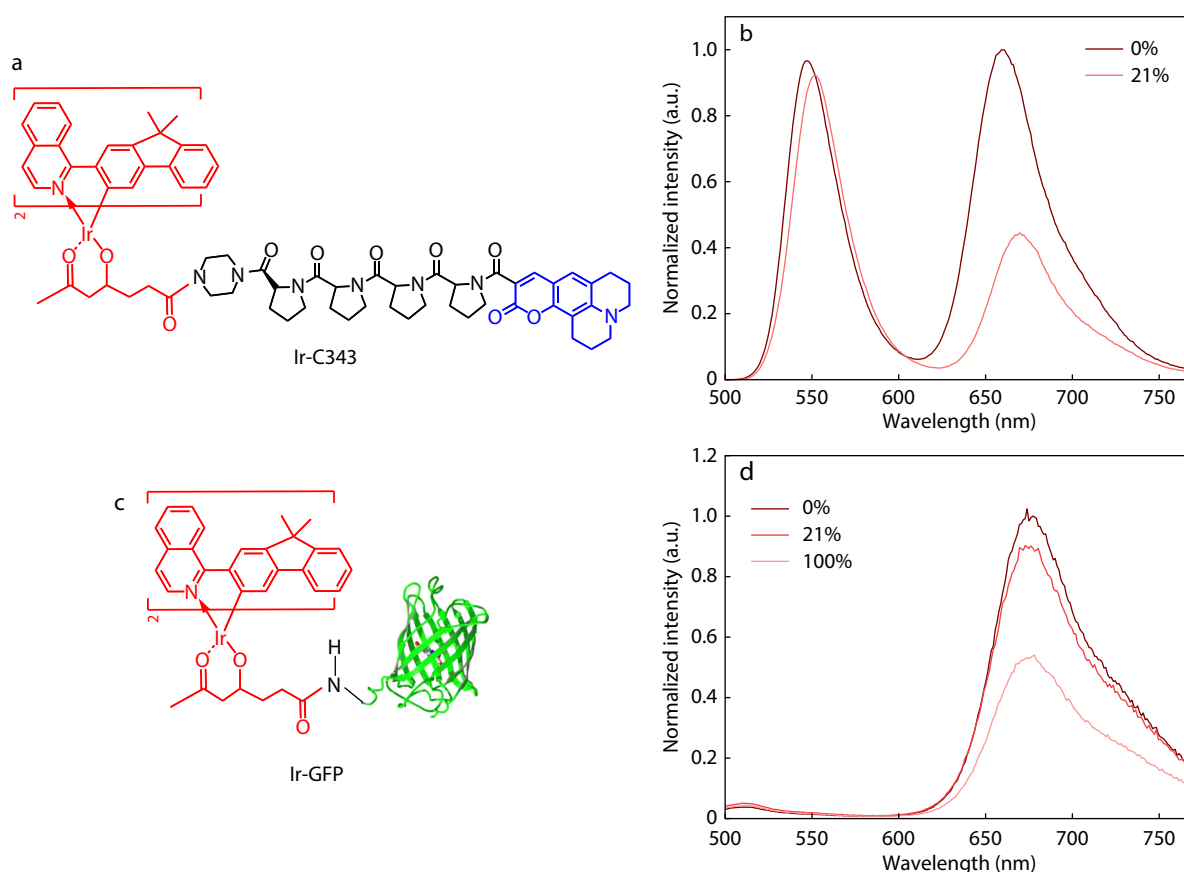The schematic diagram of the Ir-C343@F127 nanoparticles is

Fig. 1   (a) Chemical structures of Ir-C343; (b) Emission spectra of Ir-C343 in DMSO under different oxygen concentrations (hypoxia and normoxia). Excitation wavelength: 445 nm; (c) Structure of Ir-GFP; (d) Emission spectra of Ir-GFP in aqueous solution under different oxygen concentrations (0%, 21%, 100%). Excitation wavelength: 475 nm.

shown in Fig. 2(a). The morphology of the nanoparticles was investigated with transmission electron microscopy (TEM). As shown in Fig. 2(b), the Ir-C343@F127 nanoparticles were spherical with relatively uniform particle size. The average diameter of the Ir-C343@F127 nanoparticles measured by dynamic light scattering is about 30 nm (Fig. 2c).

Cytotoxicity of the Probes
We studied the cytotoxicity of Ir-C343, Ir-C343@F127 and Ir-GFP probes by MTT assay. As shown in Fig. 3(a), the Ir-C343 probe

has concentration-dependent cytotoxicity. After encapsulating it into nanoparticles with F127, the biocompatibility is significantly improved. The cytotoxicity of Ir-C343@F127 is extremely low within the test concentration range, and the cell viability is above 80%.

Similarly, the very low cell cytotoxicity against RAW264.7 cells is observed in the test concentration range of Ir-GFP (Fig. 3b), and the cell viability is above 90%, which proves that the Ir-GFP probe has good biocompatibility.
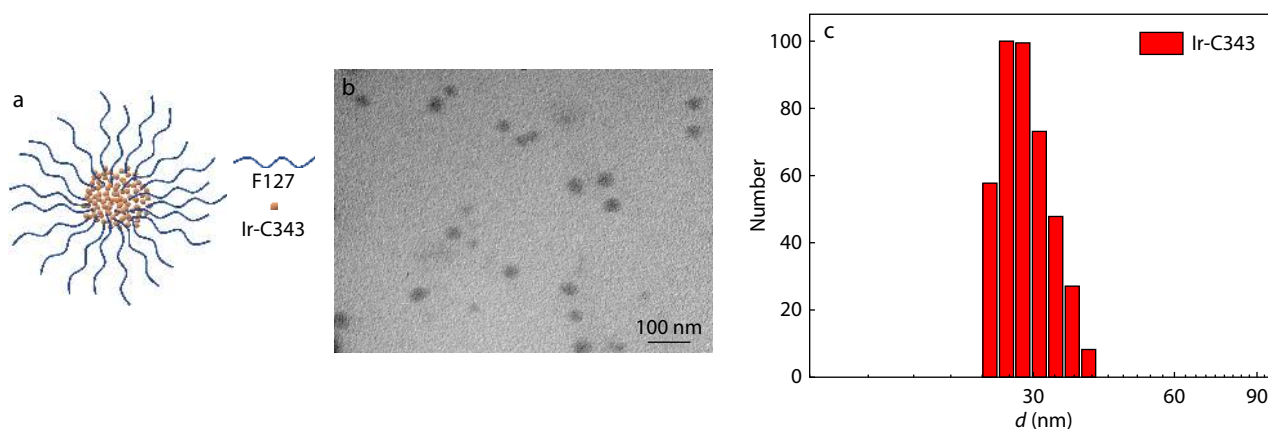

Fig. 2   (a) Schematic diagram of Ir-C343@F127 nanoparticles; (b) TEM image of Ir-C343@F127 nanoparticles; (c) Particle size distribution of Ir-C343@F127 nanoparticles.

In vitro Cell Imaging and Hypoxic Response of Ir-C343

In order to test the cell imaging ability of Ir-C343 in hypoxia, NIH3T3 cells were co-cultured with probe Ir-C343 under normoxia and hypoxia, respectively. As shown in Fig. 4(a), in different oxygen concentrations, the signal intensity of C343 channel has no much difference. The phosphorescence intensity of the Ir-fliq channel is substantially increased. Semi-quantitative analysis of the confocal images (Fig.4b) shows that the intensity ratio of phosphorescent channel can reach 2.1 under hypoxic and normoxic conditions. It can be seen that in *in vitro* cell imaging, the Ir-C343 probe can reflect the hypoxia level through the ratio imaging of the two channels. However, a
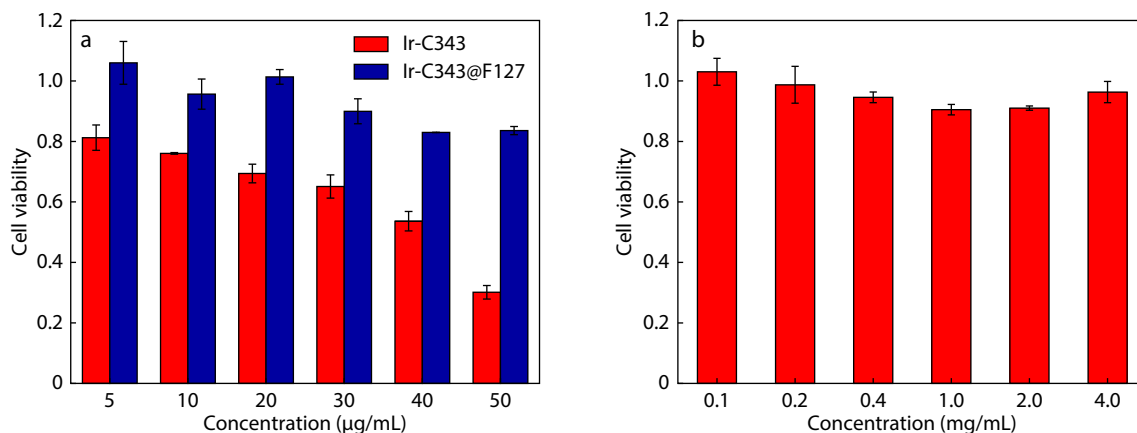

Fig. 3   (a) *In vitro* cytotoxicity of Ir-C343 and Ir-C343@F127 against RAW264.7 cells with different concentrations (5, 10, 20, 30, 40, 50 μg/mL); (b) *In vitro* cytotoxicity of Ir-GFP against RAW264.7 cells with different concentrations (0.1, 0.2, 0.4, 1, 2, 4 μg/mL).
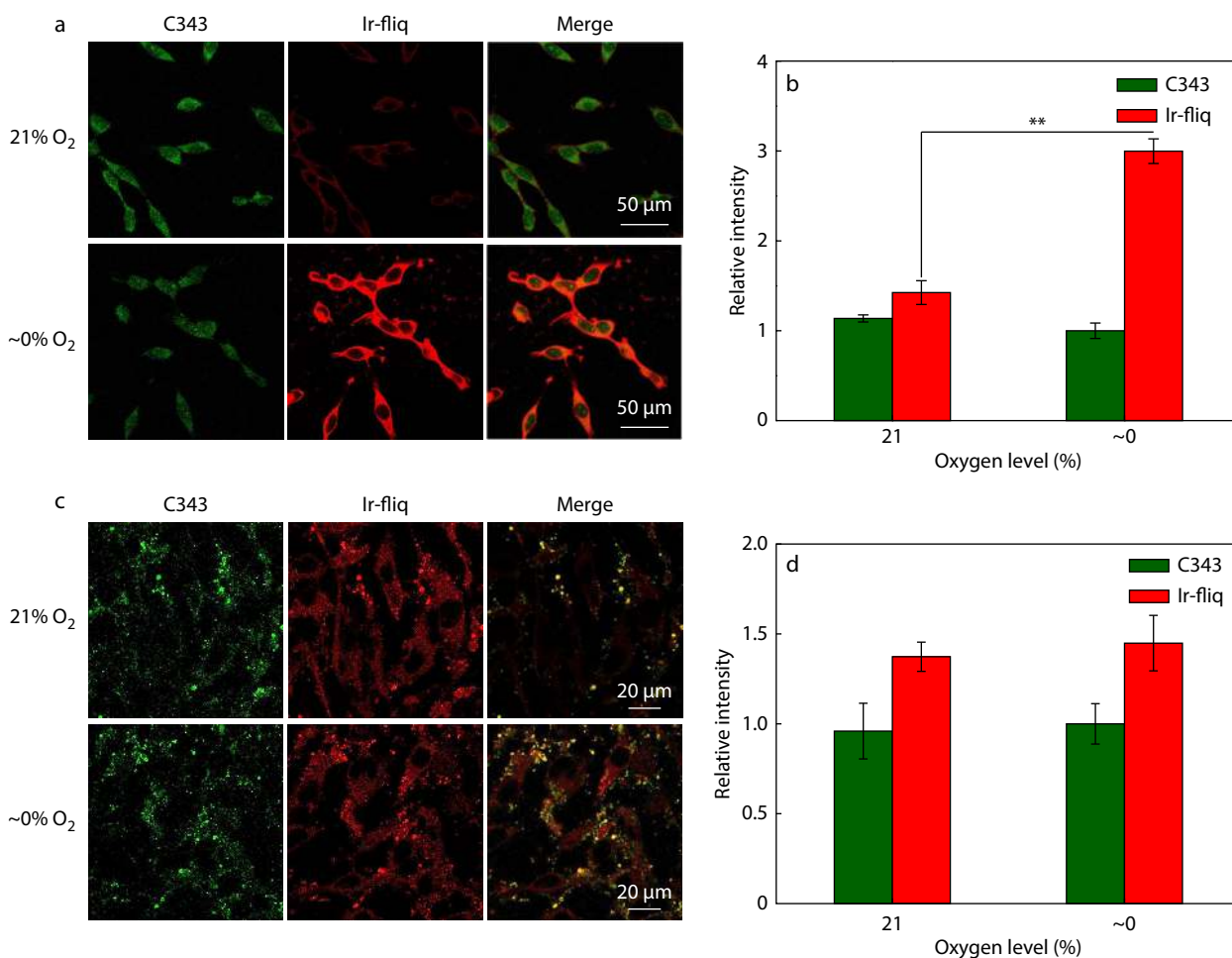

Fig. 4   *In vitro* imaging of NIH3T3 cells co-incubated with Ir-C343(a) and Ir-C343@F127(c), respectively at different oxygen concentrations; (b) Quantitative analysis of luminescence intensity in (a); (d) Quantitative analysis of luminescence intensity in (c).

phenomenon of entry into the cell nucleus of Ir-C343 was observed, and the signals of two channels were not co-localized completely. This may be associated with DMSO because Ir-C343 can only be dissolved in DMSO. Meanwhile, the MTT results showed that Ir-C343 has certain cytotoxicity. These factors will both affect the cell viability and uptake of the probe.

Next, we explored the cell imaging ability of the water-soluble nanoparticle Ir-C343@F127 under hypoxic conditions. As shown in Figs. 4(c) and 4(d), the imaging results of Ir-C343@F127 show that there is no notable difference in the intensities of the phosphorescence channel under normoxic and hypoxic environments. We infer that the formation of nanoparticles affects the contact of the Ir-fliq part with oxygen, resulting in the loss of oxygen sensitivity. Therefore, neither Ir-C343 nor Ir -C343@F127 are able to achieve ideal imaging results.

In vitro Cell Imaging and Hypoxic Response of Ir-GFP

NIH3T3 and RAW264.7 cells were co-cultured with Ir-GFP under normoxia and hypoxia, respectively. As shown in Fig. S5 (in ESI) and Fig. 5(a), the signal intensity of GFP channel has no difference between hypoxia and normoxia. Fig. 5(b) shows that the phosphorescence intensity ratio of Ir-fliq channel in

hypoxia and normoxia is about 2.3. What's more, compared with the spectral results of Ir-GFP solution, the relative intensity of the GFP channel can be found to increase significantly in the cell imaging results, which is almost close to the intensity of the Ir-fliq channel under normoxia. It indicates that compared with Ir-fliq, GFP has a more stable fluorescence and is less susceptible to the complex environment in cell imaging, demonstrating that GFP is an ideal internal standard fluorophore for biological imaging.

Tissue damage can cause inflammatory responses and lead to a variety of chronic diseases.[25] After tissue damage, innate immune cells are activated, followed by orderly infiltration of neutrophils and macrophages.[26] Macrophages are pluripotent cells with various phenotypes that have the ability to destroy and repair tissues, and play an important role in the process of repairing inflammation.[27] Therefore, a pro-inflammatory cell imaging induced by LPS and a single-cell imaging were performed to explore the metabolism and respiration of macrophages. After adding LPS solution to promote inflammation, the oxygen consumption of RAW264.7 cells were increased. As shown in Figs. 5(c) and 5(d), after LPS treatment, the signal intensity of the Ir-fliq channel is signific-
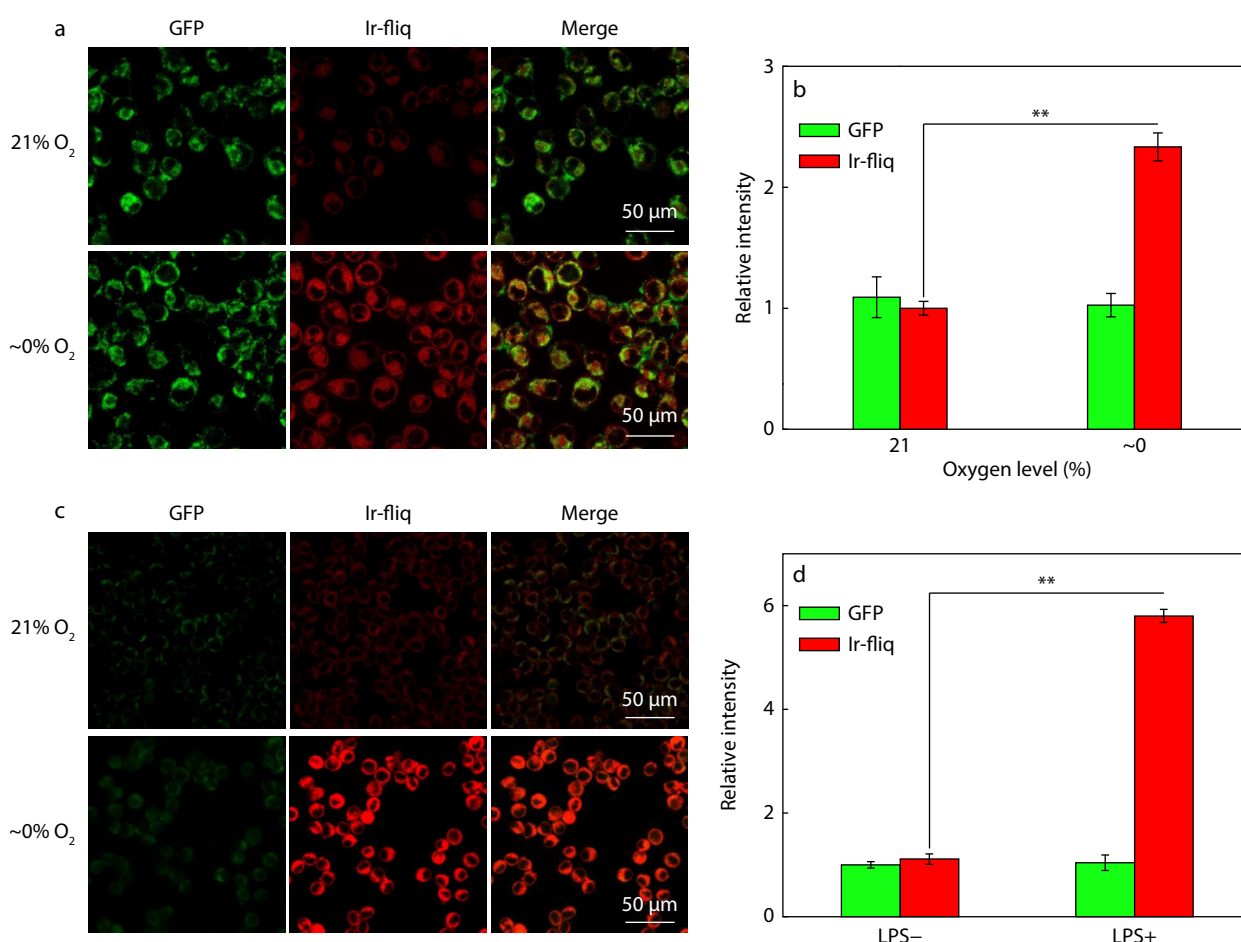

Fig. 5 (a) *In vitro* imaging of RAW264.7 cells co-incubated with Ir-GFP at different oxygen concentrations; (b) Quantitative analysis of luminescence intensity in (a); (c) *In vitro* imaging of RAW264.7 cells with/without treated by LPS; (d) Quantitative analysis of luminescence intensity in (c).

antly enhanced to 5.8 times of the untreated group. It can be seen that in *in vitro* cell imaging, the Ir-GFP probe can reflect hypoxia levels and biochemical environment in macrophages by ratiometric imaging.

Fig. 6 shows the single-cell imaging results. Since the microwells were pre-filled with the probe solution, the GFP channel can observe that each microwell has a fluorescent signal with almost the same intensity, while the Ir-fliq channel shows a completely different phenomenon. Compared with the bright field, it is found that the microwells with cells consume oxygen because of the respiration of cells, which activated the Ir-fliq signal. Due to the small diameter of RAW264.7 cells, there are two cells in single microwell in some cases, which consume more oxygen and have stronger Ir-fliq signals in these microwells (in the blue circle). For those microwells that were not loaded with cells, the solution was under normoxia and no obvious Ir-fliq signal can be observed (in the yellow circle). Fig. 6(b) shows when the number of cells in the microwells was different, the signals of GFP were almost unchanged, while the signals of Ir-fliq were significantly different. The signal in the blue and yellow circles was 1.97 and 0.42 times of that in the normal area, respectively. This result illustrates the difference in oxygen sensitivity between the two luminescent groups of the ratiometric probe Ir-GFP visually.
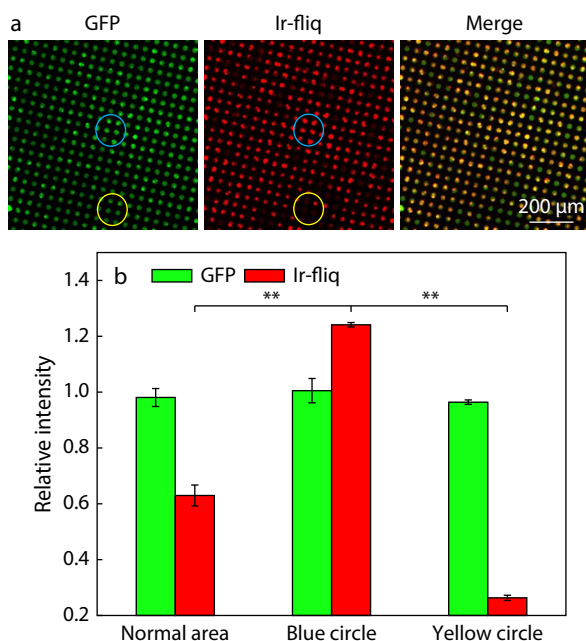

Fig. 6   (a) *In vitro* imaging of individual RAW264.7 cells co-incubated with Ir-GFP in cell-sized microwells (30 μm in diameter and height); (b) Quantitative analysis of luminescence intensity in (a).

CONCLUSIONS

In this work, two ratiometric hypoxia probes Ir-C343 and Ir-GFP based on the iridium complex Ir-fliq were successfully synthesized. After integrated with the internal standard molecule, both ratiometric probes maintain the high phosphorescence emission intensity and sensitive hypoxia response ability of Ir-fliq. Hypoxia response tests in solution and *in vitro* cell imaging show that the synthesized probes can be used for ratiometric measurement to oxygen concentrations. The fluorescence intensity of the internal standard part remains relatively constant under different oxygen concentrations, while the Ir-fliq moiety is highly sensitive to hypoxia. The ratiometric hypoxia probes can achieve a ratiometric response that is related to the oxygen concentration only and independent of probe concentration. However, the probe Ir-C343 has cytotoxicity and poor water solubility. After being coated with F127, the probe Ir-C343@F127 became unresponsive to hypoxia. The probe Ir-GFP exhibits better performance in ratiometric imaging of cells due to its longer excitation wavelength, lower fluorescence-phosphorescent relative intensity, good water solubility and better biocompatibility. This work provides the guidance of designing high-performance ratiometric hypoxic probes for cell imaging applications, and will inspire more research in this field.

NOTES

The authors declare no competing financial interest.

◆E◆ Electronic Supplementary Information

Electronic supplementary information (ESI) is available free of charge in the online version of this article at http://doi.org/10.1007/s10118-023-2922-6.

REFERENCES

1   Rudin, M.; Weissleder, R. Molecular imaging in drug discovery and development. *Nat. Rev. Drug Discov.* **2003**, *2*, 123−131.
2   Weissleder, R. Molecular imaging in cancer. *Science* **2006**, *312*, 1168−1171.
3   Lee, Y. E. K.; Kopelman, R. Optical nanoparticle sensors for quantitative intracellular imaging. *Wiley Interdiscip. Rev.-Nanomed. Nanobiotechnol.* **2009**, *1*, 98−110.
4   Li, Q.; Liu, L.; Liu, J. W.; Jiang, J. H.; Yu, R. Q.; Chu, X. Nanomaterial-based fluorescent probes for live-cell imaging. *Trac-Trends Anal. Chem.* **2014**, *58*, 130−144.
5   Smith, B. R.; Gambhir, S. S. Nanomaterials for *in vivo* Imaging. *Chem. Rev.* **2017**, *117*, 901−986.
6   Koo, H.; Huh, M. S.; Ryu, J. H.; Lee, D. E.; Sun, I. C.; Choi, K.; Kim, K.; Kwon, I. C. Nanoprobes for biomedical imaging in living systems. *Nano Today* **2011**, *6*, 204−220.
7   Wolfbeis, O. S. An overview of nanoparticles commonly used in fluorescent bioimaging. *Chem. Soc. Rev.* **2015**, *44*, 4743−68.
8   Kang, S. Y.; Wang, Y.; Xu, X. C.; Navarro, E.; Tichauer, K. M.; Liu, J. T. C. Microscopic investigation of topically applied nanoparticles for

molecular imaging of fresh tissue surfaces. *J. Biophoton.* **2018**, *11*, e201700246.

9   Leigh, S. Y.; Som, M.; Liu, J. T. C. Method for assessing the reliability of molecular diagnostics based on multiplexed SERS-coded nanoparticles. *PLoS One* **2013**, *8*, 8.

10 Wang, Y.; Reder, N. P.; Kang, S.; Glaser, A. K.; Yang, Q.; Wall, M. A.; Javid, S. H.; Dintzis, S. M.; Liu, J. T. C. Raman-encoded molecular imaging with topically applied SERS nanoparticles for intraoperative guidance of lumpectomy. *Cancer Res.* **2017**, *77*, 4506–4516.

11 Wang, Y. W.; Doerksen, J. D.; Kang, S. Y.; Walsh, D.; Yang, Q.; Hong, D.; Liu, J. T. C. Multiplexed molecular imaging of fresh tissue surfaces enabled by convection-enhanced topical staining with SERS-coded nanoparticles. *Small* **2016**, *12*, 5612–5621.

12 Papkovsky, D. B.; Dmitriev, R. I. Biological detection by optical oxygen sensing. *Chem. Soc. Rev.* **2013**, *42*, 8700–8732.

13 Tichauer, K. M.; Holt, R. W.; El-Ghussein, F.; Davis, S. C.; Samkoe, K. S.; Gunn, J. R.; Leblond, F.; Pogue, B. W. Dual-tracer background subtraction approach for fluorescent molecular tomography. *J. Biomed. Opt.* **2013**, *18*, 11.

14 Tichauer, K. M.; Wang, Y.; Pogue, B. W.; Liu, J. T. C. Quantitative *in vivo* cell-surface receptor imaging in oncology: kinetic modeling and paired-agent principles from nuclear medicine and optical imaging. *Phys. Med. Biol.* **2015**, *60*, R239–R269.

15 Haidekker, M. A.; Theodorakis, E. A. Ratiometric mechanosensitive fluorescent dyes: design and applications. *J. Mater. Chem. C* **2016**, *4*, 2707–2718.

16 Kumar, S.; Verma, T.; Mukherjee, R.; Ariese, F.; Somasundaram, K.; Umapathy, S. Raman and infra-red microspectroscopy: towards quantitative evaluation for clinical research by ratiometric analysis. *Chem. Soc. Rev.* **2016**, *45*, 1879–1900.

17 Liu, J. T. C.; Helms, M. W.; Mandella, M. J.; Crawford, J. M.; Kino, G. S.; Contag, C. H. Quantifying cell-surface biomarker expression in thick tissues with ratiometric three-dimensional microscopy. *Biophys. J.* **2009**, *96*, 2405–2414.

18 Liu, X.; Yu, Z.; Yu, M.; Zhang, X.; Xu, Y.; Lv, P.; Chu, S.; Liu, C.; Lai, W.; Huang, W. Iridium(III)-complexed polydendrimers for inkjet-printing OLEDs: the influence of solubilizing steric hindrance groups. *ACS Appl. Mater. Interfaces* **2019**, *11*, 26174–26184.

19 Jiang, Y.; Lv, P.; Pan, J.; Li, Y.; Lin, H.; Zhang, X.; Wang, J.; Liu, Y.; Wei, Q.; Xing, G.; Lai, W.; Huang, W. Low-threshold organic semiconductor lasers with the aid of phosphorescent Ir(III) complexes as triplet sensitizers. *Adv. Funct. Mater.* **2019**, *29*, 1806719.

20 Cao, S.; Hao, L.; Lai, W.; Zhang, H.; Yu, Z.; Zhang, X.; Liu, X.; Huang, W. Distinct phosphorescence enhancement of red-emitting iridium(III) complexes with formyl-functionalized phenylpyridine ligands. *J. Mater. Chem. C* **2016**, *4*, 4709–4718.

21 Liu, J.; Zhou, H.; Wang, Z.; Tang, X.; Wu, H.; Wang, S.; Lai, W.; Li, Y. Distinct Ir(III) complexes containing unsymmetric ligands with fluorene-oxadiazole groups and their performance of organic light-emitting diodes. *Dyes and Pigments* **2022**, *202*, 110252.

22 Zhang L.; Ding D. Recent advances of transition Ir(III) complexes as photosensitizers for improved photodynamic therapy. *VIEW* **2020**, *2*, 20200179.

23 Ji, S.; Zhou, S.; Zhang, X.; Chen, W.; Jiang, X. An oxygen-sensitive probe and a hydrogel for optical imaging and photodynamic antimicrobial chemotherapy of chronic wounds. *Biomater. Sci.* **2022**, *10*, 2054–2061.

24 Yoshihara, T.; Yamaguchi, Y.; Hosaka, M.; Takeuchi, T.; Tobita, S. Ratiometric molecular sensor for monitoring oxygen levels in living cells. *Angew. Chem. Int. Ed.* **2012**, *51*, 4148–51.

25 Rodrigues, M.; Kosaric, N.; Bonham, C. A.; Gurtner, G. C. Wound healing: a cellular perspective. *Physiol. Rev.* **2019**, *99*, 665–706.

26 Cooke, J. P. Inflammation and its role in regeneration and repair. *Circ. Res.* **2019**, *124*, 1166–1168.

27 Rodrigues, M.; Gurtner, G. C. Black, white, and gray: macrophages in skin repair and disease. *Curr. Pathobiol. Rep.* **2017**, *5*, 333–342.